Korean J. Chem. Eng., **18**(6), 824-830 (2001)

Development of Counter-Current Flow Limitation Model Applicable to a Sharp-Edged Liquid Entrance

Ji Hwan Jeong

Dept. of Environmental Management, Cheonan College of Foreign Studies,
Anseo-dong, Cheonan, Choongnam 330-705, Korea
(*Received 22 May 2001 • accepted 28 July 2001*)

Abstract—There are many industrial machines that function by operation of multi-phase fluids. Some of them take advantage of the characteristics of counter-current two-phase flow. The maximum flow rates of gas and liquid phases which flow in opposite-directions (counter-current flow) are limited by a phenomenon known as a Counter-Current Flow Limitation (CCFL or flooding). The mass and momentum conservation equations for two phases were established to build a system of first-order partial derivative equations (PDE). A new CCFL model was developed based on the characteristic equation of the first-order PDE system. The present model applies to the case in which a non-uniform flow is developed around a square or sharp-edged entrance of liquid phase. The model can be used to predict the operating-limit of components in which mass and heat transfer are taking place between liquid and gas phases.

Key words: CCFL, Flooding, Counter-Current Flow, Hyperbolic System, Characteristic Equation

INTRODUCTION

A large number of industrial systems adopt a counter-current two-phase flow configuration in which the gas phase flows upwards and the liquid phase downwards. In order to achieve maximum flow rates of counter-current two-phase flow with a fixed pumping power, each phase should flow separately. If a circular flow path is vertically installed, the dominant flow pattern would be an annular flow regime. Let us assume an annular flow regime in which a water film flows downwards along the inside of a circular pipe and a gas stream flows upwards along the central region surrounded by the liquid film. With low gas and liquid flow rates, two separate fluids flow preserving annular flow regime. When gas flow rate increases, the interfacial friction between two phases increases and waves are developed on the interface. Sine waves with small amplitude and various wavelengths are initially generated in the upper part of the test section. As they move downwards, the waves grow, competing with each other in absorbing the kinetic energy of gas flow. It is speculated that waves with the most dangerous wavelength (with which waves grow fastest) grow dominantly and are converted into large roll waves [Peng, 1991]. When the gas flow rate reaches a critical value, roll waves grow instantaneously, and in turn, a smooth annular flow regime can persist no longer. The flow configuration turns into a chaotic flow pattern and the penetration flow rate of the liquid phase decreases significantly. Under this situation, the liquid penetration rate does not increase even if more liquid is supplied. This transition phenomenon is called a Counter-Current Flow Limitation (CCFL) or flooding. The gas phase velocity that makes CCFL occur is called CCFL gas velocity or flooding gas velocity. With less flow rate than CCFL liquid velocity, all the water supplied to a liquid entrance penetrates the flow path. However, most of supplied liquid accumulates above the liquid entrance if flooding occurs.

†To whom correspondence should be addressed.
E-mail: jhjeong@ccfs.ac.kr

Since this characteristic of the CCFL phenomenon sets an operation limit of chemical process plants in which heat and mass transfer occur between gas and liquid phases, chemical engineers began investigating this phenomenon around five decades ago. Nowadays, chemical engineers are interested in flooding since packed columns [Han and Hong, 1998] and structured packings [Cho et al., 1995] have been widely adopted by the chemical and allied industries. Also, the CCFL phenomenon is of importance in the field of safety analysis of nuclear power plants (NPPs) as it prevents the emergency core cooling system (ECCS) of NPPs from performing its function successfully.

CCFL phenomena have been investigated in analytical as well as experimental ways so that many models have been developed. The analytical models can be categorized in three groups as follows:

(1) Wave dynamics model: based on the idea that waves are developed on a liquid film and the waves become unstable to induce CCFL phenomena. Cetinbudaklar and Jameson [1969], Richter [1981], Shearer and Davidson [1965], Wallis and Kuo [1976] models are in this group.

(2) Drop dynamics model: based on the idea that CCFL occurs when the gravity force exerted on a liquid drop is in a balance with the drag force by gas flow. Lee et al. [1982], McCarthy and Lee [1979] model are in this group.

(3) Liquid film dynamics model: The velocity distribution of a liquid film is calculated. Several models were developed at the condition that net liquid flow rate becomes zero and some models are at an instability condition of liquid film. Maron and Dukler [1984], Taitel et al. [1982], Wallis [1969], Bharathan et al. [1979] models are in this group.

Most of the CCFL models, including empirical correlations, are expressed in terms of non-dimensional parameters such as Wallis parameter and Kutateladze number:

$$j_k^* = j_k \sqrt{\frac{\rho_k}{gD(\rho_f - \rho_g)}}, \quad (1)$$

$$K_k^* = j_k \sqrt{\frac{\rho_k^2}{g\sigma(\rho_f - \rho_g)}}, \quad (2)$$

where, g, D, σ, ρ, and j denote gravitational acceleration, characteristic length, surface tension, density, and superficial velocity, respectively. The subscripts g, f, and k represent gas phase, liquid phase and arbitrary phase. It is well known that CCFL velocity is significantly influenced by geometric conditions, especially, liquid entrance and exit geometries [Jeong and No, 1994]. As it is hard to take these geometries' information into analytical models, most of the models in the literature were developed with the assumption that the flow path is circular and infinitely long. Or, in some literature, it is assumed that the smooth liquid supply and extraction to and from circular flow path acts as if the liquid phase is supplied and extracted through a porous medium [Lacy and Dukler, 1994]. In reality, however, the non-smooth geometry of a liquid entrance and exit have more wider application than a smooth one. In consequence, many empirical correlations have been developed to consider the geometry effects on CCFL and most of them are in the form of simple linear equations as follows:

$$j_g^{*1/2} + m j_f^{*1/2} = C^2 \quad (3)$$

$$K_g^{*1/2} + m K_f^{*1/2} = C^2 \quad (4)$$

There are two tuning parameters in Eqs. (3) and (4), which are known to be functions of geometric conditions of flow path. These parameters are usually tuned to fit experimental measurements.

Wallis and Kuo [1976] derived a mathematical expression that shows the interface shape of hanging film on the square edge. The results of their work give some insights into liquid behavior on a square edge. However, their formula does not seem to be appropriate for predicting CCFL occurring at a sharp-edged liquid entrance. It is because the formula is derived with an assumption that liquid film is stationary, hanging by the momentum of upward flowing gas phase. The objective of the present work is to develop an analytical CCFL model that is applicable to the geometry of sharp-edged liquid entrance around which a non-uniform flow of liquid phase develops. A model based on the concept of wave instability is developed and compared with experimental measurements.

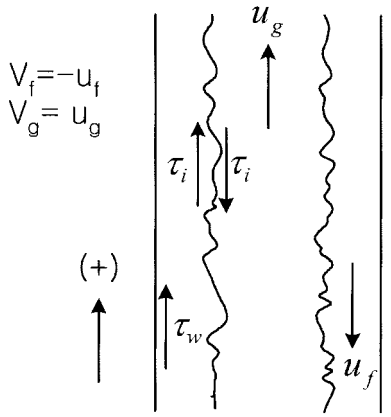

Fig. 1. Schematic of a vertical annular flow system.

ANNULAR TWO-PHASE FLOW SYSTEM

In order to develop a CCFL model, a vertical annular flow regime is assumed as schematically shown in Fig. 1. A gas phase flows upwards and liquid phase downwards. The opposite direction to gravity is set to be positive. The mass conservation equation for each phase is as follows:

Vapour mass

$$\frac{\partial}{\partial t}(\alpha_g \rho_g) + \frac{\partial}{\partial z}(\alpha_g \rho_g V_g) = 0 \quad (5)$$

Liquid mass

$$\frac{\partial}{\partial t}(\alpha_f \rho_f) + \frac{\partial}{\partial z}(\alpha_f \rho_f V_f) = 0 \quad (6)$$

where, V_g, V_f represents u_g, $-u_f$ in Fig. 1, respectively and the α_g, α_f represents void fraction, and liquid fraction, respectively.

The momentum equations of two phases are derived on the assumptions that the vapour pressure is equal to the interfacial pressure of a phase, and the spatial derivative of the pressure difference between two phases, $\Delta P = P_f - P_g$, is a function of the void fraction only. Therefore, its spatial derivative can be expressed as $\partial \Delta P/\partial z = (\partial \Delta P/\partial \alpha_g)\partial \alpha_g/\partial z$. With these assumptions, the momentum conservation equation for each phase is as follows:

Vapour momentum

$$\alpha_g \rho_g \frac{\partial V_g}{\partial t} + \alpha_g \rho_g V_g \frac{\partial V_g}{\partial z} + \alpha_g \frac{\partial P_g}{\partial z} = -4\frac{\sqrt{\alpha_g}}{D}\tau_i - \alpha_g \rho_g g \quad (7)$$

Liquid momentum

$$\alpha_f \rho_f \frac{\partial V_f}{\partial t} + \alpha_f \rho_f V_f \frac{\partial V_f}{\partial z} + \alpha_f \frac{\partial P_f}{\partial z} = 4\frac{\sqrt{\alpha_g}}{D}\tau_i - \frac{4}{D}\tau_w - \alpha_f \rho_f g \quad (8)$$

where,

$$P_f = P_g + \Delta P, \Delta P = P_f - P_g, \frac{\partial P_f}{\partial z} = \frac{\partial P_g}{\partial z} + \frac{\partial \Delta P}{\partial \alpha_g}\frac{\partial \alpha_g}{\partial z},$$

$$\tau_i = \frac{f_i}{2}\rho_g |V_g| V_g, \tau_w = \frac{f_w}{2}\rho_f |V_f| V_f.$$

The above equations are rearranged to build a system of first-order partial differential equations (PDE) as follows:

$$\underline{\underline{A}}\frac{\partial \underline{X}}{\partial t} + \underline{\underline{B}}\frac{\partial \underline{X}}{\partial z} = \underline{C} \quad (9)$$

The matrixes and vectors, $\underline{X}$, $\underline{\underline{A}}$, $\underline{\underline{B}}$, $\underline{C}$ are as follows:

$$\underline{X} = (P_g, \alpha_g, V_g, V_f)^T \quad (10)$$

$$\underline{\underline{A}} = \begin{pmatrix} \alpha_g C_g^{-2} & \rho_g & 0 & 0 \\ \alpha_f C_f^{-2} & -\rho_f & 0 & 0 \\ 0 & 0 & \alpha_g \rho_g & 0 \\ 0 & 0 & 0 & \alpha_f \rho_f \end{pmatrix} \quad (11)$$

$$\underline{\underline{B}} = \begin{pmatrix} \alpha_g V_g C_g^{-2} & \rho_g V_g & \alpha_g \rho_g & 0 \\ \alpha_f V_f C_f^{-2} & -\rho_f V_f & 0 & \alpha_f \rho_f \\ \alpha_g & 0 & \alpha_g \rho_g V_g & 0 \\ \alpha_f & \alpha_g \frac{\partial \Delta P}{\partial \alpha_g} & 0 & \alpha_f \rho_f V_f \end{pmatrix} \quad (12)$$

$$\underline{C}=\begin{pmatrix} 0 \\ 0 \\ -4\frac{\alpha_g^{1/2}}{D}\tau_i-\alpha_g\rho_g g \\ 4\frac{\alpha_g^{1/2}}{D}\tau_i-\frac{4}{D}\tau_w-\alpha_f\rho_f g \end{pmatrix} \tag{13}$$

where, $C_g^{-2}=\frac{\partial\rho_g}{\partial P_g}$, $C_f^{-2}=\frac{\partial\rho_f}{\partial P_f}$ are sonic velocity terms.

The propagation of the wave front can be expressed as a wave coordinate, ξ, defined by

$$\xi=z+\lambda t \tag{14}$$

In Eq. (14), λ means the velocity of information propagation from upstream to downstream. By transforming the coordinate (t, z) into ξ, Eq. (9) is transformed into the form of

$$(\underline{A}\lambda+\underline{B})\frac{\partial\underline{X}}{\partial\xi}=\underline{C} \tag{15}$$

After neglecting the elements with sonic velocity C_g^{-2} and C_f^{-2} which are much smaller compared with the orther terms, one can obtain the gradient of the void fraction among the gradient of $\underline{X}$.

$$\frac{\partial\alpha_g}{\partial\xi}=\frac{N(\alpha_g)}{\Delta} \tag{16}$$

where,

$$\Delta=-\alpha_f\rho_g(\lambda+V_g)^2-\alpha_g\rho_f(\lambda+V_f)^2+\alpha_g\alpha_f\frac{\partial\Delta P}{\partial\alpha_g} \tag{17}$$

$$N(\alpha_g)=4\frac{\sqrt{\alpha_g}}{D}\tau_i-\frac{4}{D}\alpha_g\tau_w-\alpha_g\alpha_f\Delta\rho g \tag{18}$$

If $\Delta\neq0$, the points in the phase space are regular points, but if $\Delta=0$, they become singular points. The propagation velocity of information, λ, obtained from the characteristic equation, $\Delta(\lambda)=0$, is all distinct and real for a hyperbolic system [Ames, 1977]. Lax [1958] proved that the requirements of well-posedness of linear PDE like Eq. (9) are the same as those of hyperbolicity. The well-posed problem guarantees the stability of its solutions. When λ becomes imaginary, the hyperbolicity breaks down, that is, the system is not hyperbolic any more. As λ means the propagation velocity of information, the imaginary part of λ means that the information of upstream cannot transfer to the downstream. In consequence, the system will move to another stable condition. Therefore, the condition of hyperbilicity breaking for a first-order PDE system represents the neutral stability condition. The CCFL phenomenon is believed to be under the same situation. When the liquid flow rate is low, the whole supplied liquid penetrates the flow path. If the liquid flow rate is below a certain critical value, the increase in the liquid supply results in the increase in the penetration flow rate. When the liquid supply reaches or exceeds the CCFL condition, most of the liquid cannot penetrate the flow path but accumulates above the liquid entrance. At the same time, annular flow regime changes into a chaotic flow pattern. This means that the information of liquid supply increase does not transfer to the downstream and the annular flow regime changes into a new stable condition of chaotic flow pattern. In this regard, the present CCFL model will be derived from the neutral stability condition.

The solution of the characteristic equation $\Delta(\lambda)=0$ is

$$\lambda=p\pm\sqrt{(p^2-q)} \tag{19}$$

where,

$$p=\frac{\alpha_f\rho_g V_g+\alpha_g\rho_f V_f}{\alpha_f\rho_g+\alpha_g\rho_f} \tag{20}$$

$$q=\frac{\alpha_f\rho_g V_g^2+\alpha_g\rho_f V_f^2+\alpha_g\alpha_f\frac{\partial\Delta P}{\partial\alpha_g}}{\alpha_f\rho_g+\alpha_g\rho_f} \tag{21}$$

The neutral stability confition is obtained by setting the square root part of Eq. (19) to zero.

$$(V_g-V_f)^2=-\frac{\partial\Delta P}{\partial\alpha_g}\frac{\alpha_f\rho_g+\alpha_g\rho_f}{\rho_g\rho_f} \tag{22}$$

Introducing superficial velocities and Wallis parameter into Eq. (22) gives

$$\frac{j_g^*}{\alpha_g}+\sqrt{\frac{\rho_g}{\rho_f}}\frac{j_f^*}{\alpha_f}=N_{ip}\sqrt{\alpha_g+\alpha_f(\rho_g/\rho_f)} \tag{23}$$

where,

$$N_{ip}=\left(-\frac{\partial\Delta P/\partial\alpha_g}{gD\Delta\rho}\right)^{1/2} \tag{24}$$

Several investigators have used this kind of approach in other areas of two-phase flow problems. Turner [1979] applied this approach to the instability of density currents and Iyer and Theofanous [1991] applied it to the thermal mixing in nuclear power plants under high pressure injection.

CCFL MODEL

In order to evaluate Eq. (24), information on the pressure difference between liquid film and gas phase is necessary. For this purpose, an ideal ring-like solitary wave as shown in Fig. 2 is considered. The wave profile is assumed to be the same as the Korteweg-de Vries's solitary wave [Drazin, 1983].

$$\delta(\xi)=h\sec h^2(\kappa\xi)+\delta_0 \tag{25}$$

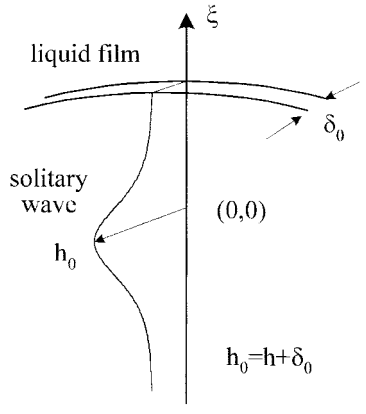

Fig. 2. Simplified solitary wave to obtain its radius of curvature.

where, δ, δ_0, h_0, κ represent film thickness, thickness of substrate, film height at the center of the solitary wave ($h+\delta_0$), and wave number ($2\pi/\lambda_w$), respectively. The gas velocity reaches the maximum at the peak of a solitary wave; in consequence, gas phase pressure reaches the minimum by Bernoulli's equation. Therefore, it can be assumed that a solitary wave becomes unstable from the peak. The pressure difference between two phases reaches the maximum at the peak of the wave and is described as follows:

$$\Delta P = \sigma\left(\frac{1}{R_1}+\frac{1}{R_2}\right) \text{ at } \xi=0 \tag{26}$$

where,

$$R_1 = R-(h+\delta_0) \tag{27}$$

$$R_2 = \left(\frac{-\partial^2\delta/\partial\xi^2}{[1+(\partial\delta/\partial\xi)^2]^{3/2}}\bigg|_{\xi=0}\right)^{-1} \approx \left(-\frac{\partial^2\delta(\xi)}{\partial\xi^2}\bigg|_{\xi=0}\right)^{-1} = \frac{1}{2h\kappa^2} \tag{28}$$

In the above equations, R represents the radius of flow path and $1/R_1$, $1/R_2$ denote the radius of curvatures of a solitary wave in azimuthal and length directions, respectively. In most cases, $1/R_1$ is much smaller than $1/R_2$, so that $1/R_1$ can be neglected safely. Then, Eq. (26) becomes

$$\Delta P = 2\sigma\kappa^2(h_0-\delta_0) \tag{29}$$

The relation between void fraction at the peak and wave height is $\alpha_g=(1-2h_0/D)^2$. Sustituting this relation into Eq. (29) and differentiating ΔP with respect to α_g, we can get an expression for $\partial\Delta P/\partial\alpha_g$. Substituting this expression and $\kappa=2\pi/\lambda_w$ into Eq. (24) gives

$$N_{ip} = \frac{1}{\sqrt{2}}\sqrt{\frac{\sigma}{g\Delta\rho}}\frac{2\pi}{\lambda_w}\alpha_g^{-1/4} \tag{30}$$

It is assumed that the wavelength of the solitary wave is the same as that of the faster growing wave at marginal Helmholtz instability. That is, $\lambda_w=2\pi\sqrt{\sigma/g\Delta\rho}$. This assumption means that a solitary wave will lose its stability by Helmholtz instability. Substituting this wavelength formula and Eq. (30) into Eq. (23) and neglecting the second term in the square root, the following simplified form is obtained.

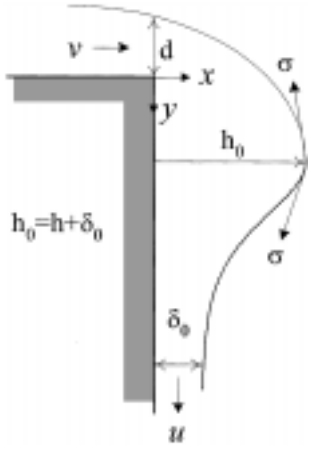

Fig. 3. Schematic of a non-uniform flow around a rectangular liquid entrance.

$$j_g^* = \frac{1}{\sqrt{2}}\alpha_g^{5/4} - \frac{\alpha_g}{\alpha_f}\sqrt{\frac{\rho_g}{\rho_f}}j_f^* \tag{31}$$

where, α_g denotes the void fraction at the peak of the wave. In order to use Eq. (31) to predict CCFL occurrence, information of void fraction or liquid fraction is required.

In this work, a square liquid entrance is selected as shown in Fig. 3, which shows the left half of the cross sectional view of a circular flow path. The liquid phase flows horizontally and later vertically downwards. A non-uniform flow develops around the entrance to make a force balance between horizontal momentum of liquid flow and surface tension force. This horizontal force balance can be expressed as follows:

$$\frac{1}{2}\rho_f v^2 = \sigma\left(\frac{1}{R_1}+\frac{1}{R_2}\right) \tag{32}$$

This force balance equation is established to calculate the liquid fraction at the peak of the non-uniform flow. The $1/R_1$, $1/R_2$ denote the radius of curvature of azimuthal and vertical directions of the non-uniform flow. Since $1/R_2$ is much larger than $1/R_1$, $1/R_1$ can be neglected in Eq. (32). As there is not a funtion that describes the surface shape of the non-uniform flow availabe, an assumption to calculate $1/R_2$ is necessary. It is assumed that $1/R_2$ is proportional to the height, h. Then,

$$\frac{1}{2}\rho_f v^2 \approx \sigma\frac{1}{R_2} = \sigma C_1 h \tag{33}$$

In the horizontal flow region, liquid phase velocity (v) and depth (d) are in relation of $v=\sqrt{gd}$, and liquid volume flow rate per unit length of periphery is $q_f=v\cdot d$. Combining these relations, we get a relation between liquid velocity and volume flow rate.

$$v = (gq_f)^{1/3} \tag{34}$$

Combining Eqs. (33), (34), and $Q_f=\pi Dq_f$, we get

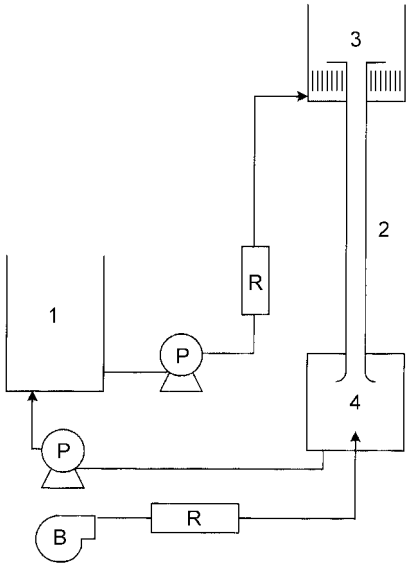

Fig. 4. Schematic diagram of experimental apparatus.

1. Water reservoir
2. Test section
3. Upper plenum
4. Lower plenum

B. Air blower
P. Pump
R. Flow meter

$$h=\frac{\rho_f}{2\sigma C_1}\left(\frac{gD}{4}\right)^{2/3}\left(\frac{gD\Delta\rho}{\rho_f}\right)^{1/3} j_f^{*2/3} \quad (35)$$

Since the liquid fraction of symmetrical annular flow can be approximated as $\alpha_f \cong 4h/D$, Eq. (36) is rearranged to give liquid fraction as follows:

$$\alpha_f=\frac{g\rho_f}{\sigma C_1}\left(\frac{1}{4}\right)^{1/6}\left(\frac{\Delta\rho}{\rho_f}\right)^{1/3} j_f^{*2/3} \quad (36)$$

EXPERIMENTAL APPARATUS

The experimental measurements were made in order to prove the applicability of the present CCFL model. A schematic diagram of the experimental loop is shown in Fig. 4. Air and de-mineralized water are used as working fluids. The apparatus consists of an upper plenum, a lower plenum and a test section connecting both of them; all of them are made of acrylic resin to allow visual observations. The test section is a circular pipe of which length and inner diameter are 100 cm and 3 cm, respectively. A horizontal circular plate of 430 mm in diameter is installed at the upper end of the test section to simulate a square liquid entrance. The lower end is machined to be round in order to minimize the interaction between air flowing into and water coming out of test section. A 7 hp blower supplies air. The supplied air to the lower plenum goes to the test section via a honeycomb type flow distributor in order to make the air flow even. The lower plenum and the distributor also play the role of damper to an air pressure fluctuation. The water is pumped to the bottom of the upper plenum from a reservoir, and flows upward via a honeycomb type flow distributor to make the water flow uniform. The water penetrating the test section is accumulated in the lower plenum, and the water level in the lower plenum is kept constant by controlling the returning flow rate to the reservoir. As the loop is closed, the thermal energy by pumping work is continuously added to the water during runs. In order to get rid of the energy and keep the water temperature at a constant level, a heat exchanger made of a helical copper tube is installed in the reservoir. The occurrence of CCFL is noticed by visual observations and the flow rates of two phases are measured by rotameters.

RESULTS AND DISCUSSION

In this experiment, the CCFL point is reached by setting the water flow rate at a constant level and step-wisely increasing the air flow rate. In the range of high water flow rate, a non-uniform flow develops around a sharp-edged liquid entrance. When the air flow rate reaches a certain level, the smooth non-uniform flow bursts into a chaotic flow pattern and the water penetration reduces significantly. This change of flow regime happens instantaneously so that the occurrence of CCFL is noticed easily by visual observation. Jeong and No [1996] referred to this kind of CCFL as entrance flooding since the flooding is initiated near the liquid phase entrance. In the range of low water flow rate, CCFL is initiated around the liquid exit even though a non-uniform flow develops around the liquid entrance. It is because the peak of the non-uniform flow is lower than that of solitary wave developed on the liquid film around the liquid exit. That is, the solitary waves developed on the liquid film around the liquid exit become unstable earlier than the non-uniform flow does. This kind of CCFL was referred to as exit flooding since the flooding is initiated near the liquid phase exit. The present model is only applicable to prediction of the entrance flooding since the present flooding model, Eq. (31), was derived based on the characteristics of non-uniform flow developing around a sharp-edged liquid entrance.

The liquid fraction at the peak of a non-uniform flow, Eq. (36), needs to be identified in order to use Eq. (31) in predicting CCFL occurrence. The liquid fraction measurements made by Jeong and No [1996] were used in developing a semi-empirical correlation. They measured liquid fraction in test sections of which i.d. are 2, 3, 4, and 5 cm. In their experiments, a CCD camera is vertically installed above the upper plenum in alignment with the test section

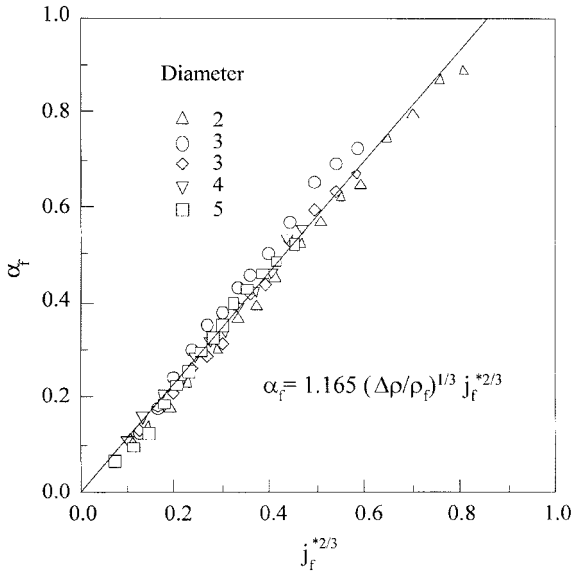

Fig. 5. Liquid fraction at the peak of non-uniform flow.

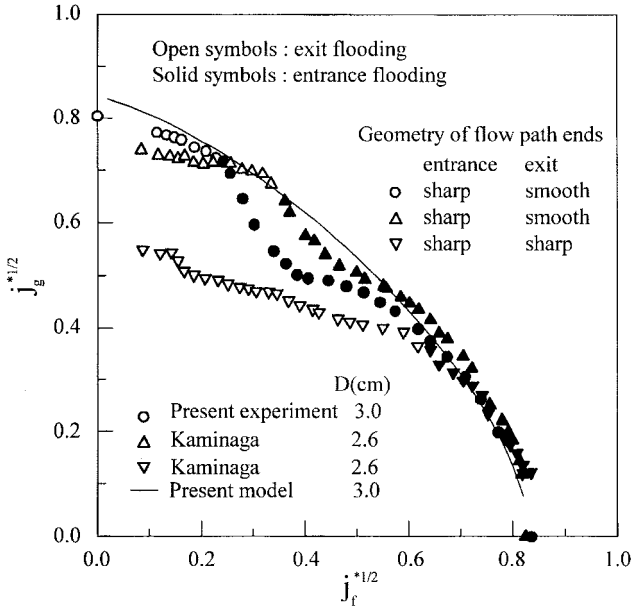

Fig. 6. Comparisons among present model and experimental measurements.

to capture the images of non-uniform flow. The images were processed on a personal computer with graphic software to calculate the liquid fraction at the peak of non-uniform flow. Fig. 5 shows the measurements and a line made by regression analysis. A semi-empirical liquid fraction model that follows Eq. (36) was found to be as follows:

$$\alpha_f = 1.165\left(\frac{\Delta\rho}{\rho_f}\right)^{1/3} j_f^{*2/3}, \quad (j_f^{*2/3} < 0.8) \tag{37}$$

Eq. (37) is the same form as Kaminaga et al.'s [1991] empirical correlation of which the proportional coefficient is 1.143. They measured the liquid fraction of non-uniform flow by visual observation and fit the measurements without physical rationale.

The prediction by the present model and measurements are compared in Fig. 6. Kaminaga et al.'s [1991] measurements are also compared in this plot. The solid line in Fig. 6 represents the prediction by Eq. (31) and (37) for 3 cm i.d. circular pipe. There are solid symbols (●, ▲ and ▼) as well as open symbols (○, △ and ▽) for the same shapes in Fig. 6. The solid symbols represent the occurrence of entrance flooding occurring at the non-uniform flow developed around the sharp-edged liquid entrance. The prediction by the present model and experimental measurements made by Kaminaga et al. [1991] as well as those by the present work are in good agreement in the range of high water flow rate. The open symbols represent the occurrence of exit flooding occurring around the liquid exit. These data points are out of the scope of the present model since the present model has its application to the entrance flooding occurring at the sharp-edged liquid phase entrance.

The circular symbols (○, ●) denote the present measurements in a 3 cm i.d. test section. The regular and inverted triangles (△, ▲, ▽ and ▼) denote Kaminaga et al.s measurements made in 2.6 cm i.d. circular pipe. The geometry of the test section for regular triangle points (△, ▲) is the same as the present experiments. The liquid phase entrance and exit of them are sharp-edged and smoothly curved, respectively. However, the geometry of the both ends for the inverted triangle points (▽, ▼) is sharp-edged. In this case, the interaction between water coming out of and air coming into the test section becomes very energetic near the liquid exit. In other words, much perturbation is introduced into the liquid film at around liquid exit. Therefore, CCFL phenomena may start to happen at the liquid exit before the non-uniform flow at the entrance loses its stability. Whether entrance flooding occurs or exit flooding occurs depends on the liquid flow rate. The entrance flooding and the exit flooding compete with each other to take place according to the liquid and gas flow rates. Flooding will occur at the place where liquid phase loses its stability first. If liquid flow rate is large, the peak height of the non-uniform flow developed near liquid entrance is larger than the wave heights of solitary waves developed on the falling liquid film so that the non-uniform flow loses its stability earlier. If liquid flow rate is small, the peak height of the non-uniform flow is smaller than the wave height of the solitary wave fully developed near the liquid exit so that falling liquid film near the exit loses its stability earlier. In this regard, it can be stated that entrance flooding (▼) occurs when the liquid phase flow rate is large, while exit flooding (▽) occurs when the liquid flow rate is small. The same situation happens in the cases where the geometry of the liquid exit is smoothly curved (○, ●, △ and ▲). When liquid flow rate is small, CCFL initiates at the liquid exit even if the liquid entrance is square. It is because the peak of a solitary wave fully developed on the falling liquid film can be higher than that of the non-uniform flow developed at the entrance. In these cases, however, a possible perturbation introduced into the liquid film is relatively small because the liquid exit is smoothly curved. It means that entrance flooding prevailing region is wider than the previous case. More detailed phenomenological observation is described in Jeong and No [1996]. This physical fact is considered to cause the discrepancy between the exit flooding data and the present model in Fig. 6.

CONCLUDING REMARKS

An analytical model for CCFL prediction is developed from the characteristic equation of a two-fluid equation system. The basic idea is that a solution to the characteristic equation represents the velocity of information transport. If the solution has an imaginary part, the information of the upstream does not propagate to the downstream. The CCFL occurs under this situation. That is, the increase in liquid supply to the upstream does not result in the increase in liquid penetration flow rate but accumulates in the upper plenum when CCFL occurs.

This model is applicable to prediction of CCFL occurring where the liquid entrance is sharp so that non-uniform flow develops around it. In order to use this model to predict the CCFL occurrence by non-uniform flow instability, the liquid fraction model for the peak of the non-uniform flow is developed. The parametric structure was derived by an analytical method and a proportional coefficient was determined by experimental measurements. Analytical CCFL models applicable to the geometry of sharp-edged liquid entrance were rare in the literature. Due to this circumstance, the comparison of adequacy between the present model and other models was not made. Only the comparisons among the present model, the present measurements, and other investigator's measurements show that the present model is in good agreement with experimental data.

NOMENCLATURE

C : constant
D : diameter
f : friction coefficient
g : gravitational acceleration
j_k : non-dimensional superficial velocity of k-phase
j_k^* : Wallis' parameter $[j_k\sqrt{\rho_k/gD(\rho_f-\rho_g)}]$
K_k^* : Kutateladze number $[j_k\sqrt{\rho_k^2/g\sigma(\rho_f-\rho_g)}]$
m : constant
P : pressure
t : time
V, u : velocity

Greek Letters

α : average volume fraction
δ : film thickness
κ : wave number
λ : information propagation velocity

λ_w : wave length by Helmholtz instability
ρ : density
σ : surface tension
τ_i : interfacial friction
ξ : wave coordinate ($\xi=z+\lambda t$)

Subscripts

g : gas phase
f : liquid phase
i : interface
w : wall

REFERENCES

Ames, W. F., "Numerical Methods for Partial Differential Equations," Academic Press (1997).

Bharathan, D., Wallis, G. B. and Richter, H. J., "Air-Water Countercurrent Annular Flow," EPRI Report, NP-1165 (1979).

Cetinbudaklar, A.G . and Jameson, G. J., "The Mechanism of Flooding in Vertical Countercurrent Two-Phase Flow, Chemical Engineering Science 24," 1669 (1969).

Cho, S. Y., Lee, Y. Y. and Kim, S. J., "A Study on Characteristics of a Modern Structured Packing," *Korean J. Chem. Eng.*, **12**, 313 (1995).

Drazin, P. G., "Solitions, Lecture Note Series 85," London Mathematical Society (1983).

Han, D. H. and Hong, W. H., "Reactive Extraction of Lactic Acid in a Packed Column," *Korean J. Chem. Eng.*, **15**, 324 (1998).

Iyer, K. and Theofanous, T. G., "Flooding-Limited Thermal Mixing: the Case of High Froude Number Injection," *Nuclear Science Engineering*, **108**, 198 (1991).

Jeong, J. H. and No, H. C., "Classification of Flooding Data According to Type of Tube-End Geometry," *Nuclear Engineering Design*, **148**, 109 (1994).

Jeong, J. H. and No, H. C., "Experimental Study of the Effect of Pipe Length and Pipe-End Geometry on Flooding," *Int. J. Multiphase Flow*, **22**, 499 (1996).

Kaminaga, F., Okamoto, Y. and Shibata, Y., "Evaluation of Entrance Geometry Effect on Flooding," Proc. 1st JSME/ASME Joint Int. Conference On Nucl. Eng., Tokyo, 95 (1991).

Lacy, C. E. and Dukler, A. E., "Flooding in Vertical Tubes-II: A Film Model for Entry Region Flooding," *Int. J. Multiphase Flow*, **20**, 235 (1994).

Lax, P. D., "Differential Equations, Difference Equations and Matrix Theory," Comm. Pure Appl. Math. XI, 174 (1958).

Lee, H. M., MaCarthy, G. E. and Tien, C. L., "Liquid Carry-over and Entrainment in Air-Water Countercurrent Flooding," EPRI Report, NP-2344 (1982).

MaCarthy, G. E. and Lee, H. M., "Review of Entrainment Phenomena and Application to Vertical Two-Phase Countercurrent Flooding," EPRI Report, NP-1284 (1979).

Maron, D. Moalem and Dukler, A. E., "Flooding and Upward Film Flow in Vertical Tubes-II: Speculations on Film Flow Mechanisms," *Int. J. Multiphase Flow*, **10**, 599 (1984).

Peng, C. A., Jurman, L. A. and McCready, M. J., "Formulation of Solitary Waves on Gas-Sheared Liquid Layers," *Int. J. Multiphase Flow*, **17**, 767 (1991).

Richter, H. J., "Flooding in Tubes and Annuli," *Int. J. Multiphase Flow*, **7**, 647 (1981).

Shearer, C. J. and Davidson, J. F., "The Investigation of a Standing Wave Due to Gas Blowing Upwards over a Liquid Film; Its Relation to Flooding in Wetted-Wall Columns," *J. of Fluid Mechanics*, **22**, 321 (1965).

Taitel, Y., Barnea, D. and Dukler, A. E., "A Film Model for the Prediction of Flooding and Flow Reversal for Gas-Liquid Flow in Vertical Tubes," *Int. J. Multiphase Flow*, **8**, 1 (1982).

Turner, J. S., "Buoyancy Effects in Fluids," Cambridge University Press (1979).

Wallis, G. B., "One Dimensional Two-Phase Flow," McGraw Hill (1969).

Wallis, G. B. and Kuo, J. T., "The Behavior of Gas-Liquid Interfaces in Vertical Tubes," *Int. J. Multiphase Flow*, **2**, 521 (1976).